Research Square

Preprints are preliminary reports that have not undergone peer review.
They should not be considered conclusive, used to inform clinical practice,
or referenced by the media as validated information.

Dynamics of dispersion of coaxial SH-waves in a pre-stressed piezo cylindrical column, with ideal and non-ideal coatings of epoxy graphite, zinc and isotropic layers

Mohammad Arif
Vellore Institute of Technology University
Parvez Alam
alamparvez.amu@gmail.com
Vellore Institute of Technology University
Tabinda Nahid
Vellore Institute of Technology University
Manoj Kumar Singh
Magadh University

Research Article

Keywords: SH-waves, Piezoelectric, Orthotropic, Transversely isotropic, Isotropic, Non-ideal interface, Prestress, Phase velocity

Posted Date: August 11th, 2026

DOI: https://doi.org/10.21203/rs.3.rs-10490229/v1

License: This work is licensed under a Creative Commons Attribution 4.0 International License.
Read Full License

Additional Declarations: No competing interests reported.

Dynamics of dispersion of coaxial SH-waves in a pre-stressed piezo cylindrical column, with ideal and non-ideal coatings of epoxy graphite, zinc and isotropic layers

Mohammad Arif[1], Parvez Alam*[1] and Tabinda Nahid[1], and Manoj Kumar Singh[2]
Department of Mathematics, School of Advanced Sciences,
[1]Vellore Institute of Technology, Vellore-632014, TN, India
[2]P.G. Department of Mathematics, Magadh University, Bodh Gaya, 824234, Bihar, India
* Corresponding Author; E-mail: alamparvez.amu@gmail.com

July 26, 2026

Abstract

In this study, propagation of circumferential SH-waves in a composite cylindrical column consisting of a pre-stressed piezoelectric core surrounded by perfectly and imperfectly bonded layers has been studied. For this purpose, three different types of coating materials, namely, epoxy graphite (orthotropic), zinc (transversely isotropic), and isotropic materials have been considered. Inclusion of imperfect interface is done to make the model more practical since it accounts for the physical and mechanical discontinuity at the interface of adjacent layers. The governing equations have been established in cylindrical coordinates based on electromechanical interaction, material anisotropy, and initial stress. Analytical solution has been obtained employing the method of separation of variables resulting in Bessel function solutions. Dispersion equation for SH-wave propagation is developed using the boundary and imperfect interface conditions. Results have been illustrated numerically to analyse the impact of piezoelectric constant, dielectric constant, initial stress, and radius ratio on phase velocity for the chosen coating materials under perfect and imperfect interface conditions. It has been found that these parameters affect the dispersion properties and the phase velocity increases with an increase in their values.

Keywords

SH-waves; Piezoelectric; Orthotropic; Transversely isotropic; Isotropic; Non-ideal interface; Pre-stress; Phase velocity

1 Introduction

Piezoelectric materials fall within the class of smart materials that show electromechanical coupling, whereby mechanical force results in electrical polarization while electrical force causes mechanical deformation. This phenomenon, referred to as the piezoelectric effect, was first reported by Jacques and Pierre Curie in 1880 [1]. The origin of this behavior lies in the absence of centrosymmetry in their crystal structures, which enables efficient energy conversion between mechanical and electrical domains [2]. Based on material composition, piezoelectric materials are generally classified as natural, ceramic, and polymeric. Naturally occurring piezoelectrics, such as quartz and Rochelle salt, inherently exhibit piezoelectricity [3]. Ceramic materials, including lead zirconate titanate (PZT) and barium titanate ($BaTiO_3$), are widely employed

owing to their large piezoelectric coefficients, thermal stability, and tunable electromechanical properties [4]. In contrast, polymer-based piezoelectrics, particularly polyvinylidene fluoride ($PVDF$), are valued for their flexibility, low density, and suitability for wearable and biomedical applications [5].

Owing to these advantageous properties, piezoelectric materials have found extensive applications across industrial, medical, and technological domains. In industrial settings, they are commonly used in pressure sensors, accelerometers, and active vibration control systems [6]. Medical applications include ultrasonic imaging devices, dental instruments, and targeted drug delivery systems [7]. Additionally, piezoelectric materials play a significant role in vibration-based energy harvesting, where ambient mechanical energy is converted into electrical power for low-energy electronic devices [8]. Their utilization also extends to aerospace and defense technologies, such as sonar systems, adaptive structures, and vibration damping mechanisms [9]. Recent research trends emphasize the development of flexible piezoelectric films for wearable electronics and soft robotics [10], piezoelectric nanogenerators based on ZnO and GaN nanostructures [11], and high-temperature piezoceramics for operation in extreme environments [12]. Furthermore, growing interest in environmentally sustainable technologies has motivated the exploration of lead-free piezoelectric alternatives, including KNN and BNT systems, along with their integration into emerging AI- and IoT-enabled platforms [13].

The propagation of shear-horizontal (SH) waves in piezoelectric structures has attracted considerable attention due to its relevance in sensing, nondestructive evaluation, and acoustic device design. TaiSong Li and YanHong Wang [14] studied the circumferential propagation of SH waves in the piezoelectric cylindrical rod with the imperfect orthotropic layer covering. In the current study, their's model is extended to three types of coatings such as orthotropic, transversely isotropic, and isotropic ones, and also the effect of perfect and imperfect bonding between layers is considered. Related investigations include the work of Jiang et al. [15], who analyzed magneto–elastic coupled wave propagation around cylindrical cavities in exponentially graded piezomagnetic media. Alam et al. [16] examined radial harmonic wave propagation in cylindrical shells composed of orthotropic, transversely isotropic, and isotropic materials under combined magnetic and hydrostatic effects. Pankaj et al. [17] explored polarized SH-wave propagation in a pre-stressed piezoelectric cylinder coated with a self-reinforced layer, while Arif and Alam [18] studied dispersion and damping characteristics of SH- waves in a piezoelectric–viscoelastic cylindrical structure with an imperfect interface. More recently, Pengpeng et al. [19] evaluated the magneto-electro-elastic response of functionally graded piezoelectric–piezomagnetic cylindrical and spherical shells under symmetric loading conditions, and Alam et al. [20] analyzed SH-wave dispersion in functionally graded piezomagnetic cylindrical structures incorporating interface imperfections. Seema et al. [21] investigated the transmission of shear-horizontal waves in prestressed rotating piezoelectric-piezomagnetic cylinders with imperfect interfaces, employing analytical modeling and parametric analysis. Wang et al. [22] studied the scattering of antiplane shear waves by a piezoelectric circular cylinder with an imperfect interface.

Transversely isotropic materials constitute an important subclass of anisotropic solids characterized by isotropic mechanical behavior within a plane and distinct properties along the direction normal to that plane [23]. Such symmetry simplifies the constitutive description, requiring only five independent elastic constants to represent the stress–strain relationships [24]. Common examples include fiber-reinforced composites, stratified rocks, wood, and certain crystalline materials, where microstructural alignment induces directional dependence of mechanical response [25]. These materials are extensively employed in engineering and geophysical modeling, as they effectively capture the behavior of layered or laminated media that are isotropic in-plane but anisotropic through the thickness [26]. In wave propagation studies, transversely isotropic models are particularly important because the symmetry axis strongly influences dispersion and attenuation characteristics [27]. A thorough understanding of their elastic response offers valuable insights into stress distribution, energy dissipation, and the dynamic stability of

composite systems [28]. Alam et al. [29] analyzed Love-type wave propagation in a transversely isotropic layer subjected to magnetic and hydrostatic stresses over an inhomogeneous half-space, employing Green's function and Fourier transform techniques. Abd-alla et al. [30] investigated the role of initial stress on magnetoelastic flexural wave propagation in a transversely isotropic circular cylinder.

A thorough numerical study has been done in this paper for studying the SH-wave propagation problem in a two-layer composite cylinder where one layer is made of piezoelectric material and the other layer is made of circumferentially transeversisotropic material. The effect of different dimensional parameters such as piezoelectric parameter (e_{15}^{II}), dielectric parameter (ε_{11}^{II}), initial stress in outer layer (χ_{rr}^{II}) and radii ratio (a/b) on the phase velocities and attenuation factors of SH-waves has been investigated. The coupling between the mechanical field and the electric field in piezoelectric material and the influence of anisotropy and imperfect interface govern the dispersion behavior of SH-waves in composite materials. The present numerical study can reveal some interesting aspects of wave propagation in composite cylindrical structure.

2 Mathematical Formulation and Solution

In the current study, the problem of propagation of SH-waves is considered in a solid cylindrical composite made up of a pre-strained piezoelastic cylinder of radius b and coated with an initially strained transversely isotropic material layer of thickness $(a-b)$, as shown in Fig. 1. An imperfect interface between the two different mediums is assumed. A cylindrical coordinate system (r, Θ, z) is utilized for formulation and solution of the problem.

Denoting u_r^i, u_Θ^i, and u_z^i as the displacement components in the radial r-, circumferential Θ-, and axial z-directions, respectively, where $(i = I, II)$, corresponds to the respective medium. For the propagation of SH-waves in the circumferential Θ-direction, it is assumed that there is an axial shear deformation in the composite structure. Thus, the displacement components are assumed in such a manner that radial and circumferential displacement components are zero whereas the axial displacement component exists. In this way, the displacement components are assumed to be

$$u_r^i = u_\Theta^i = 0, \quad u_z^i = u_z^i(r, \Theta, t) \quad \text{and} \quad \frac{\partial}{\partial z} \equiv 0; \quad i = I, II. \tag{1}$$

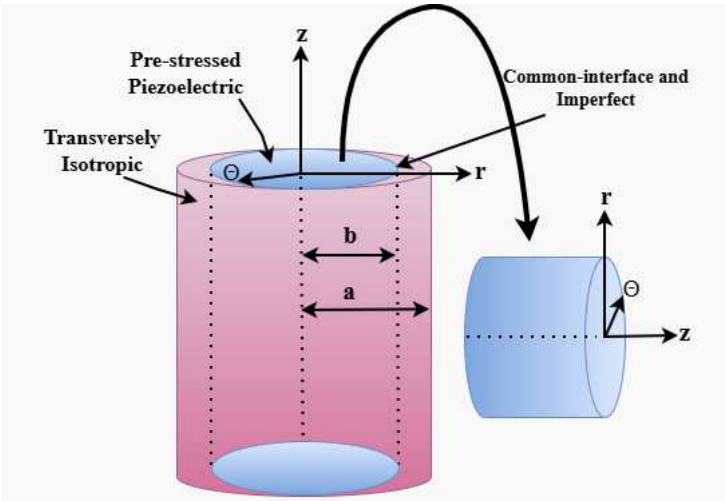


Figure 1: Considered Geometry of the problem

Following Biot's theory, the equations of motion for an elastic solid without initial stress are obtained [31].

$$\frac{\partial \Pi_{rz}^I}{\partial r} + \frac{1}{r}\frac{\partial \Pi_{\Theta z}^I}{\partial \Theta} + \frac{\Pi_{rz}^I}{r} = \rho^I \frac{\partial^2 u_z^I}{\partial t^2}, \tag{2}$$

where Π_{ij} denotes the components of the stress tensor, ρ^I represents the mass density of the medium.

The stress–strain relations for the mechanical response of the material, based on Hooke's law, are written as:

(i) For orthotropic media, the corresponding stress–strain relations are given by:

$$\begin{aligned}
\Pi_{rr}^I &= \alpha_{11}^I \xi_{rr} + \alpha_{12}^I \xi_{\Theta\Theta} + \alpha_{13}^I \xi_{zz}, \quad \Pi_{rz}^I = \alpha_{44}^I \xi_{rz} \\
\Pi_{\Theta\Theta}^I &= \alpha_{12}^I \xi_{rr} + \alpha_{22}^I \xi_{\Theta\Theta} + \alpha_{23}^I \xi_{zz}, \quad \Pi_{\Theta z}^I = \alpha_{55}^I \xi_{\Theta z} \\
\Pi_{zz}^I &= \alpha_{13}^I \xi_{rr} + \alpha_{23}^I \xi_{\Theta\Theta} + \alpha_{33}^I \xi_{zz}, \quad \Pi_{r\Theta}^I = \alpha_{66}^I \xi_{r\Theta}
\end{aligned}$$

For a transversely isotropic material, the constitutive stress–strain relations simplify due to material symmetry, such that $\alpha_{11} = \alpha_{22}$, $\alpha_{23} = \alpha_{31}$, $\alpha_{44} = \alpha_{55}$, and $\alpha_{66} = (\alpha_{11} - \alpha_{12})/2$. Accordingly, the stress components are expressed as:

$$\begin{aligned}
\Pi_{rr} &= \alpha_{11} \xi_{rr} + \alpha_{12} \xi_{\Theta\Theta} + \alpha_{13} \xi_{zz}, \quad \Pi_{rz} = \alpha_{44} \xi_{rz} \\
\Pi_{\Theta\Theta} &= \alpha_{12} \xi_{rr} + \alpha_{11} \xi_{\Theta\Theta} + \alpha_{13} \xi_{zz}, \quad \Pi_{\Theta z} = \alpha_{44} \xi_{\Theta z} \\
\Pi_{zz} &= \alpha_{13} \xi_{rr} + \alpha_{13} \xi_{\Theta\Theta} + \alpha_{33} \xi_{zz}, \quad \Pi_{r\Theta} = \alpha_{66} \xi_{r\Theta}
\end{aligned}$$

(iii) In the special case of isotropic materials, the elastic constants reduce to $\alpha_{11} = \alpha_{22} = \alpha_{33} = \lambda + 2\mu$, $\alpha_{12} = \alpha_{13} = \alpha_{23} = \lambda$, and $\alpha_{44} = \alpha_{55} = \alpha_{66} = \mu$, where λ and μ are the Lamé constants. The corresponding stress–strain relations are given by:

$$\begin{aligned}
\Pi_{rr} &= (\lambda + 2\mu) \xi_{rr} + \lambda \xi_{\ominus\Theta} + \lambda \xi_{zz}, \quad \Pi_{rz} = \mu \xi_{rz} \\
\Pi_{\Theta\Theta} &= \lambda \xi_{rr} + (\lambda + 2\mu) \xi_{\ominus\Theta} + \lambda \xi_{zz}, \quad \Pi_{\Theta z} = \mu \xi_{\Theta z} \\
\Pi_{zz} &= \lambda \xi_{rr} + \lambda \xi_{\ominus\Theta} + (\lambda + 2\mu) \xi_{zz}, \quad \Pi_{r\Theta} = \mu \xi_{r\Theta}
\end{aligned}$$

where, $\xi_{rr} = \frac{\partial u_r^I}{\partial r}$, $\xi_{\Theta\Theta} = \left(\frac{1}{r}\frac{\partial u_\Theta^I}{\partial \Theta} + \frac{u_r^I}{r}\right)$, $\xi_{zz} = \frac{\partial u_z^I}{\partial z}$, $\xi_{rz} = \left(\frac{\partial u_z^I}{\partial r} + \frac{\partial u_r^I}{\partial z}\right)$, $\xi_{r\Theta} = \left(\frac{1}{r}\frac{\partial u_r^I}{\partial \Theta} + \frac{\partial u_\Theta^I}{\partial r} + \frac{u_\Theta^I}{r}\right)$ and $\xi_{\Theta z} = \left(\frac{\partial u_\Theta^I}{\partial z} + \frac{1}{r}\frac{\partial u_z^I}{\partial \Theta}\right)$.

In view of Hook's law, Eq. (2) yields

$$\alpha_{44}^I \frac{\partial^2 u_z^I}{\partial r^2} + \frac{\alpha_{55}^I}{r^2}\frac{\partial^2 u_z^I}{\partial \Theta^2} + \frac{\alpha_{44}^I}{r}\frac{\partial u_z^I}{\partial r} = \rho^I \frac{\partial^2 u_z^I}{\partial t^2}. \tag{3}$$

Taking the solution of Eq. (3) as $u_z^I(r, \Theta, z) = V^I(r) \exp[(k\Theta - \omega t)i]$, hence Eqn. (3) takes the form

$$\frac{d^2 V^I}{dr^2} + \frac{1}{r}\frac{dV^I}{dr} + \left(l^2 - \frac{\nu^2}{r^2}\right) V^I = 0, \tag{4}$$

where, $l = \sqrt{\frac{\rho^I \omega^2}{\alpha_{44}^I}}$ and $\nu = k\sqrt{\frac{\alpha_{55}^I}{\alpha_{44}^I}}$.

Above Eqn. (4) is the known Bessel's differential equation and its general solution is given by

$$V^I(r) = \mathfrak{I}_1 J_\nu(lr) + \mathfrak{I}_2 Y_\nu(lr), \tag{5}$$

$\mathfrak{I}_1$ and $\mathfrak{I}_2$ are arbitrary constants, whereas $J_\nu(lr)$ and $Y_\nu(lr)$ denote the first and second kinds of order k, respectively.

The expression for the displacement component (u_z^I) is determined by

$$u_z^I(r, \Theta, z) = [\mathfrak{I}_1 J_\nu(lr) + \mathfrak{I}_2 Y_\nu(lr)] \exp[(k\Theta - \omega t)i] \tag{6}$$

3 Piezoelectric Medium

Following [9], the governing equations for a piezoelectric cylinder subjected to radial initial stress are written as

$$\left.\begin{array}{l} \frac{\partial \Pi_{rz}^{II}}{\partial r}+\frac{1}{r}\frac{\partial \Pi_{\Theta z}^{II}}{\partial \Theta}+\frac{\Pi_{rz}^{II}}{r}+\left(\frac{1}{r^2}\frac{\partial^2 v^{II}}{\partial \Theta^2}+\frac{1}{r}\frac{\partial v^{II}}{\partial r}+\frac{\partial^2 v^{II}}{\partial r^2}\right)\chi_{rr}^{II}=\rho^{II}\frac{\partial^2 v^{II}}{\partial t^2}, \\ \frac{\partial \Omega_r^{II}}{\partial r}+\frac{1}{r}\frac{\partial \Omega_\Theta^{II}}{\partial \Theta}+\frac{\Omega_r^{II}}{r}=0, \end{array}\right\} \tag{7}$$

where Π_{ij}^{II} denotes the components of the stress tensor, Ω_i^{II} represents the electrical displacement, ρ^{II} is the mass density, v^{II} is the mechanical displacement along the z-direction, and χ_{rr}^{II} corresponds to the radial component of the initial stress.

The constitutive relations governing the coupled electromechanical behavior of the piezoelectric medium are expressed as

$$\Pi_{\Theta z}^{II}=\frac{1}{r}\left(\alpha_{44}^{II}\frac{\partial v^{II}}{\partial \Theta}+e_{15}^{II}\frac{\partial \varphi^{II}}{\partial \Theta}\right),\quad \Pi_{rz}^{II}=\left(\alpha_{44}^{II}\frac{\partial v^{II}}{\partial r}+e_{15}^{II}\frac{\partial \varphi^{II}}{\partial r}\right)$$
$$\Omega_r^{II}=\left(e_{15}^{II}\frac{\partial v^{II}}{\partial r}-\varepsilon_{11}^{II}\frac{\partial \varphi^{II}}{\partial r}\right)\ \text{and}\quad \Omega_\Theta^{II}=\frac{1}{r}\left(e_{15}^{II}\frac{\partial v^{II}}{\partial \Theta}-\varepsilon_{11}^{II}\frac{\partial \varphi^{II}}{\partial \Theta}\right),$$

where φ^{II} denotes the electric potential function, and α_{44}^{II}, e_{15}^{II}, and ε_{11}^{II} represent the elastic, piezoelectric, and dielectric constants of the piezoelectric medium, respectively.

Using Eqs. (7), the following coupled field equations are obtained:

$$\left.\begin{array}{l} \left(\alpha_{44}^{II}+\chi_{rr}^{II}\right)\nabla^2 v^{II}+e_{15}^{II}\nabla^2\varphi^{II}=\rho^{II}\frac{\partial^2 v^{II}}{\partial t^2}, \\ e_{15}^{II}\nabla^2 v^{II}-\varepsilon_{11}^{II}\nabla^2\varphi^{II}=0, \end{array}\right\} \tag{8}$$

where $\nabla^2=\left(\frac{\partial^2}{\partial r^2}+\frac{1}{r}\frac{\partial}{\partial r}+\frac{1}{r^2}\frac{\partial^2}{\partial \Theta^2}\right)$ denotes the two-dimensional Laplacian operator in cylindrical coordinates.

Let us introduce an auxiliary function,

$$\psi^{II}=\varphi^{II}-v^{II}\left(\frac{e_{15}^{II}}{\varepsilon_{11}^{II}}\right). \tag{9}$$

Using Eq. (9) in Eq. (8), we get

$$\left(\tilde{\alpha}_{44}^{II}+\chi_{rr}^{II}\right)\nabla^2 v^{II}=\rho^{II}\frac{\partial^2 v^{II}}{\partial t^2}\quad \text{and}\quad \nabla^2\psi^{II}=0, \tag{10}$$

where, $\tilde{\alpha}_{44}^{II}=\left[\alpha_{44}^{II}+\frac{\left(e_{15}^{II}\right)^2}{\varepsilon_{11}^{II}}\right]$.

We seek harmonic solutions of Eq. (10) in the following form:

$$v^{II}(r,\Theta,z)=V^{II}(r)\exp[(k\Theta-\omega t)i],\quad \psi^{II}(r,\Theta,z)=\tilde{\psi}^{II}(r)\exp[(k\Theta-\omega t)i], \tag{11}$$

where $V^{II}(r)$ and $\tilde{\psi}^{II}(r)$ are unknown radial functions, k denotes the wave number, and ω represents the angular frequency.

Substituting the assumed harmonic solutions from Eq. (11) into Eq. (10) yields

$$\frac{d^2V^{II}}{dr^2}+\frac{1}{r}\frac{dV^{II}}{dr}+\left(h^2-\frac{k^2}{r^2}\right)V^{II}=0, \tag{12}$$

where, $h^2=\frac{\rho^{II}\omega^2}{\tilde{\alpha}_{44}^{II}+\chi_{rr}^{II}}$.

Equation (12) reduces to a Bessel differential equation of order n, and its general solution can be expressed as

$$V^{II} = \mathfrak{I}_3 J_k(hr) + \mathfrak{I}_4 Y_k(hr), \tag{13}$$

where $\mathfrak{I}_3$ and $\mathfrak{I}_4$ are arbitrary constants, and J_n and Y_n denote the Bessel functions of the first and second kinds, respectively.

On inserting the expressions given in Eq. (11) into Eq. (10), we obtain

$$\frac{d^2\tilde{\psi}^{II}}{dr^2} + \frac{1}{r}\frac{d\tilde{\psi}^{II}}{dr} - \frac{k^2}{r^2}\tilde{\psi}^{II} = 0. \tag{14}$$

Equation (14) takes the form of a second-order Cauchy–Euler differential equation, whose solution can be written as

$$\tilde{\psi}^{II} = \mathfrak{I}_5 r^k + \mathfrak{I}_6 r^{-k}, \tag{15}$$

where, $\mathfrak{I}_5$ and $\mathfrak{I}_6$ are unknown.

The mechanical displacement and the electric potential are required to remain finite at the center of the piezoelectric core, that is, ψ^{II} and V^{II} must be bounded as $r \to 0$. Accordingly, by utilizing Eqs. (7), (9), (10), (12) and (15), the admissible expressions for the displacement field and the electric potential are obtained as

$$v^{II} = \mathfrak{I}_3 J_k(hr) \exp\left[(k\Theta - \omega t)\, i\right]. \tag{16}$$

$$\varphi^{II} = \left[\mathfrak{I}_5 r^k + \mathfrak{I}_3 \left(\frac{e_{15}^{II}}{\varepsilon_{11}^{II}}\right) J_k(hr)\right] \exp\left[(k\Theta - \omega t)\, i\right]. \tag{17}$$

4 The Boundary conditions of the problem

The following equations will serve as boundary conditions for the problem:

1. $\left(\varphi^{II}\right)_{r=b} = 0$
2. $\left(\Pi_{rz}^{I}\right)_{r=a} = 0$
3. $\left(\Pi_{rz}^{II} - \Pi_{rz}^{I}\right)_{r=b} = 0$
4. $\left[\Pi_{rz}^{II} - \beta_{ij}\left(v^I - v^{II}\right)\right]_{r=b} = 0, \quad \text{where} \quad \beta_{ij} = \frac{1}{\vartheta_{ij}}$

Interface stiffness factor β_{ij} represents the character of interaction of the two media at their interface. If the interface is perfectly bonded, then there is no discontinuity of displacement across the interface; that is, $v^I = v^{II}$, meaning $\beta_{ij} \to \infty$ (or alternatively, $\vartheta_{ij} \to 0$). If the interface is imperfectly bonded, there will be some finite discontinuity in displacement. The interfacial shear stress Π_{rz}^{II} is proportional to this displacement discontinuity; thus, $\Pi_{rz}^{II} = \beta_{ij}\left(v^I - v^{II}\right)$. Finite value of the interfacial stiffness implies imperfect bonding, while low value of the stiffness implies weak bonding.

5 Frequency Equation

By applying the prescribed boundary and interface conditions, the following set of algebraic equations is obtained:

$$\left(\frac{e_{15}^{II}}{\varepsilon_{11}^{II}}\right) J_k(hb)\mathfrak{I}_3 + b^k\, \mathfrak{I}_5 = 0. \tag{18}$$

$$\left[J_{\nu-1}(al) - J_{\nu+1}(al)\right]\mathfrak{I}_1 + \left[Y_{\nu-1}(al) - Y_{\nu+1}(al)\right]\mathfrak{I}_2 = 0. \tag{19}$$

$$[J_{\nu-1}(lb) - J_{\nu+1}(lb)]\left(\frac{\alpha_{44}^{I}l}{2}\right)\mathfrak{I}_1 + [Y_{\nu-1}(lb) - Y_{\nu+1}(lb)]\left(\frac{\alpha_{44}^{I}l}{2}\right)\mathfrak{I}_2 + h\,[J_{k+1}(hb) - J_{k-1}(hb)]\left(\frac{(e_{15}^{II})^2 + \alpha_{44}^{II}\varepsilon_{11}^{II}}{2\varepsilon_{11}^{II}}\right)\mathfrak{I}_3 - k\,b^{k-1}\frac{e_{15}^{II}}{\varepsilon_{11}^{II}}\mathfrak{I}_5 = 0. \tag{20}$$

$$-\beta_{ij}J_{\nu}(lb)\,\mathfrak{I}_1 - \beta_{ij}Y_{\nu}(lb)\,\mathfrak{I}_2 + \left\{h\,[J_{k-1}(hb) - J_{k+1}(hb)]\left[\frac{(e_{15}^{II})^2 + \alpha_{44}^{II}\varepsilon_{11}^{II}}{2\varepsilon_{11}^{II}}\right] + k\,b^{k-1}\frac{e_{15}^{II}}{\varepsilon_{11}^{II}}\right\}\mathfrak{I}_3 + k\,b^{k-1}\mathfrak{I}_5 = 0. \tag{21}$$

After simplifying the above Eqs. (19) and (20) with the help of Eq. (17), we can get the following homogeneous algebraic system of equations for unknowns $\mathfrak{I}_1$, $\mathfrak{I}_2$, and $\mathfrak{I}_3$.

$$[J_{\nu-1}(al) - J_{\nu+1}(al)]\,\mathfrak{I}_1 + [Y_{\nu-1}(al) - Y_{\nu+1}(al)]\,\mathfrak{I}_2 = 0. \tag{22}$$

$$\frac{\alpha_{44}^{I}l}{2}\,[J_{\nu-1}(lb) - J_{\nu+1}(lb)]\,\mathfrak{I}_1 + \frac{\alpha_{44}^{I}l}{2}\,[Y_{\nu-1}(lb) - Y_{\nu+1}(lb)]\,\mathfrak{I}_2 + \left[h\,(J_{k+1}(hb) - J_{k-1}(hb))\left(\frac{(e_{15}^{II})^2 + \alpha_{44}^{II}\varepsilon_{11}^{II}}{2\varepsilon_{11}^{II}}\right) + \frac{k(e_{15}^{II})^2}{b\varepsilon_{11}^{II}}J_k(hb)\right]\mathfrak{I}_3 = 0. \tag{23}$$

$$-\beta_{ij}J_{\nu}(lb)\mathfrak{I}_1 - \beta_{ij}Y_{\nu}(lb)\mathfrak{I}_2 + \left[h\,(J_{k-1}(hb) - J_{k+1}(hb))\left(\frac{(e_{15}^{II})^2 + \alpha_{44}^{II}\varepsilon_{11}^{II}}{2\varepsilon_{11}^{II}}\right) + \beta_{ij}J_k(hb) - \frac{k(e_{15}^{II})^2}{b\varepsilon_{11}^{II}}J_k(hb)\right]\mathfrak{I}_3 = 0. \tag{24}$$

For a non-trivial solution to exist, the determinant of the coefficient matrix associated with the above system must vanish, which yields the frequency equation governing wave propagation in the considered cylindrical model.

$$|\theta_{ij}| = 0; \qquad i,j = 1,2,3 \tag{25}$$

where,

$$\theta_{11} = J_{k-1}(la) - J_{k+1}(la),$$

$$\theta_{12} = Y_{k-1}(la) - Y_{k+1}(la),$$

$$\theta_{13} = 0,$$

$$\theta_{21} = \frac{\alpha_{44}^{I}l}{2}\,[J_{k-1}(lb) - J_{k+1}(lb)]\,,$$

$$\theta_{22} = \frac{\alpha_{44}^{I}l}{2}\,[Y_{k-1}(lb) - Y_{k+1}(lb)]\,,$$

$$\theta_{23} = h\,[J_{k+1}(hb) - J_{k-1}(hb)]\left(\frac{(e_{15}^{II})^2 + \alpha_{44}^{II}\varepsilon_{11}^{II}}{2\varepsilon_{11}^{II}}\right) + \frac{k(e_{15}^{II})^2}{b\varepsilon_{11}^{II}}J_k(hb),$$

$$\theta_{31} = -\beta_{ij}J_k(lb),$$

$$\theta_{32} = -\beta_{ij}Y_k(lb),$$

$$\theta_{33} = h\,[J_{k-1}(hb) - J_{k+1}(hb)]\left(\frac{(e_{15}^{II})^2 + \alpha_{44}^{II}\varepsilon_{11}^{II}}{2\varepsilon_{11}^{II}}\right) + \left[\beta_{ij} - \frac{k(e_{15}^{II})^2}{b\varepsilon_{11}^{II}}\right]J_k(hb).$$

6 Validation

If we are amusing that the initial stress is not available in the system, i.e., $P^{II} = \chi^{II}_{rr}/\alpha^{II}_{44} = 0$, then our frequency equation is matching with the frequency equation obtain by TaiSong Li and YanHong Wang [14].

7 Discussion of Numerical analysis

To examine the influence of key dimensionless parameters viz. the piezoelectric constant e^{II}_{15}, dielectric constant ε^{II}_{11}, initial stress in the inner piezoelectric cylinder ($P^{II} = \chi^{II}_{rr}/\alpha^{II}_{44}$) and the radii ratio b/a on circumferential SH-waves in a composite cylindrical column consisting of a pre-stressed piezoelectric core surrounded by perfectly and imperfectly bonded layers has been studied. For this purpose, three different types of coating materials, namely, epoxy graphite (orthotropic), zinc (transversely isotropic), and isotropic materials have been considered (Table 1). The effects of these parameters on the wave characteristics are illustrated in Figs. 2–7. Figure 8 plotted to compare the phase velocity of the waves that propagate in epoxy-graphite, zinc, and isotropic coatings for imperfect and perfect interface conditions. The material properties employed in the numerical examples of coated layer are given in Table 1 and numerical examples of Piezo column . The fixed parameter values adopted for graphical representation are listed in Table 3.

Table 1: **Numerical constants of coating layer**

Medium	Rigidity ($\times 10^{10}$ N/m^2)	Density (kg/m^3)
Epoxy graphite [27]	$\alpha^{I}_{44} = 0.361, \quad \alpha^{I}_{44} = 0.565$	1590
Zinc [32]	$\alpha^{I}_{44} = 3.96$	7140
Isotropic [33]	$\mu = 3.23$	2802

Table 2: **Numerical constants of Piezo-electric column**

Medium	Rigidity ($\times 10^{10}$ N/m^2)	Density (kg/m^3)
Piezoelectric [9, 34]	$\alpha^{II}_{44} = 2.56$ $e^{II}_{15} = 13.5$ C/m^2 $\varepsilon^{II}_{11} = 17.1 \times 10^{-9}$ F/m	7500

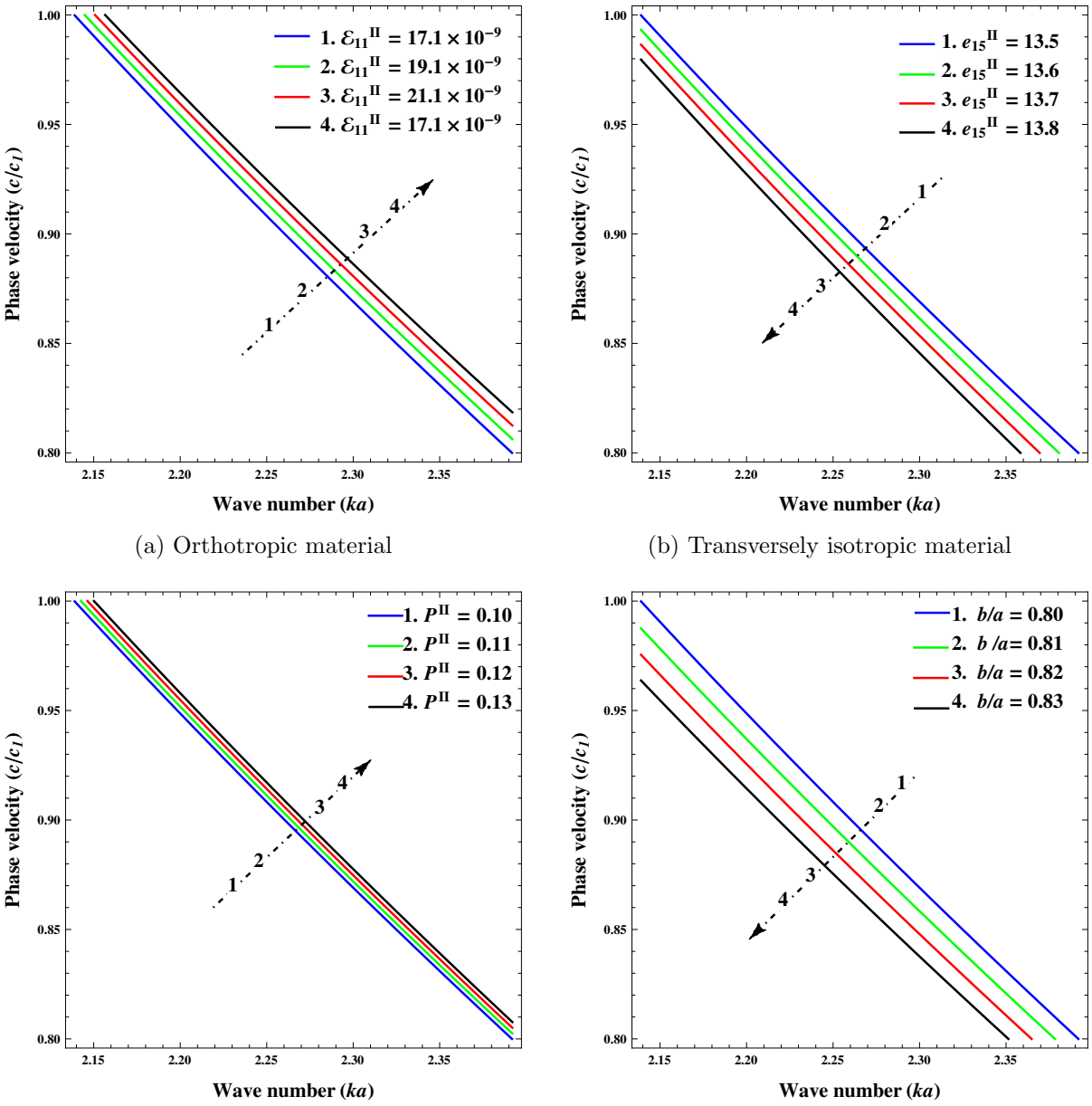
Table 3: **Fixed values of parameters**

Parameters	ε^{II}_{11}	e^{II}_{15}	P^{II}	b/a
Figure 2	-	13.5	0.10	0.80
Figure 3	17.1×10^{-9}	-	0.10	0.80
Figure 4	17.1×10^{-9}	13.5	-	0.80
Figure 5	17.1×10^{-9}	13.5	0.10	0.80
Figure 6	17.1×10^{-9}	13.5	0.10	-
Figure 7	17.1×10^{-9}	13.5	0.10	0.80

"-" denotes the parameter being varied in the corresponding figure.

7.1 Effects on the phase velocity for epoxy-graphite imperfect coating

The influence of (a) the dielectric parameter (ε^{II}_{11}), (b) the piezoelectric constant (e^{II}_{15}), (c) the initial stress (P^{II}), and (d) the radii ratio (b/a) on the phase velocity of SH-waves in the case



(a) Orthotropic material

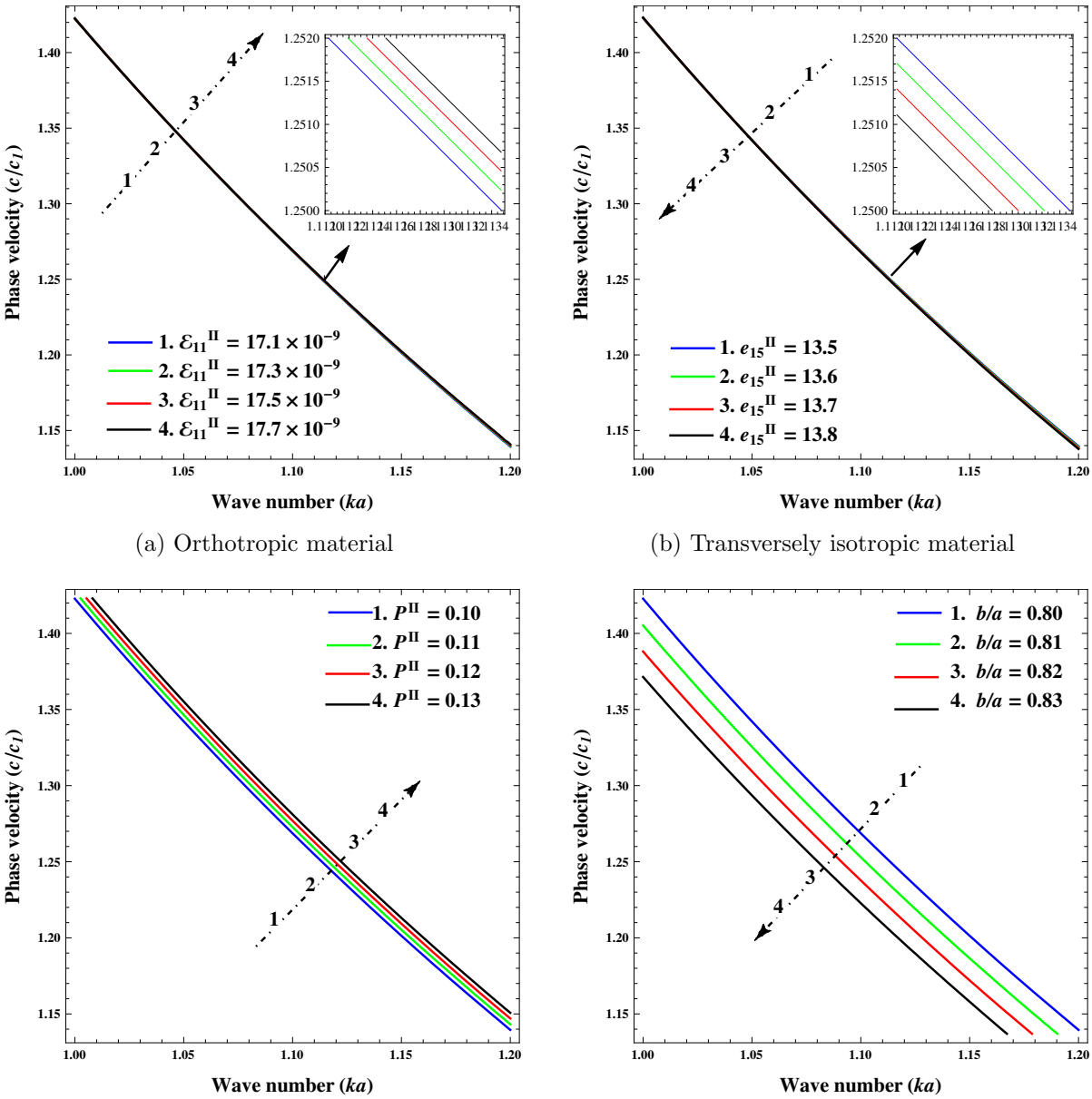
(b) Transversely isotropic material

(c) Isotropic material

(d) Comparison of all materials

Figure 2: Phase velocity variation (c/c_1) versus wave number (ka) in the case of imperfect interfaces, an orthotropic (epoxy-graphite) coating for different values of (a) dielectric constant (ε_{11}^{II}), (b) piezoelectric constant (e_{15}^{II}), (c) initial stress (P^{II}), and (d) radii ratio (b/a).

of an imperfectly bonded orthotropic coating consisting of epoxy graphite can be seen in Figure 2. In figures 2(a) and 2(c), the phase velocity of SH-wave shows an increase in its value as the values of the piezoelectric constant and initial stress are increased. The reason behind the enhancement in phase velocity with an increase in (e_{15}^{II}) is the enhanced electromechanical coupling effect, which allows better transmission of mechanical energy through the piezoelectric medium, thereby increasing the stiffness of the medium. On the other hand, it is shown in Figures 2(b) and 2(d) that the phase velocity becomes small with the rise in both the dielectric constant and radii ratio. An increase in the value of dielectric constant causes an increase in the energy storage capability of the material due to which the electromechanical coupling strength gets diminished. Likewise, the increase in the value of radii ratio results in the increase in the thickness of the coated layer; therefore, the path for the propagation of waves becomes long as



(a) Orthotropic material

(b) Transversely isotropic material

(c) Isotropic material

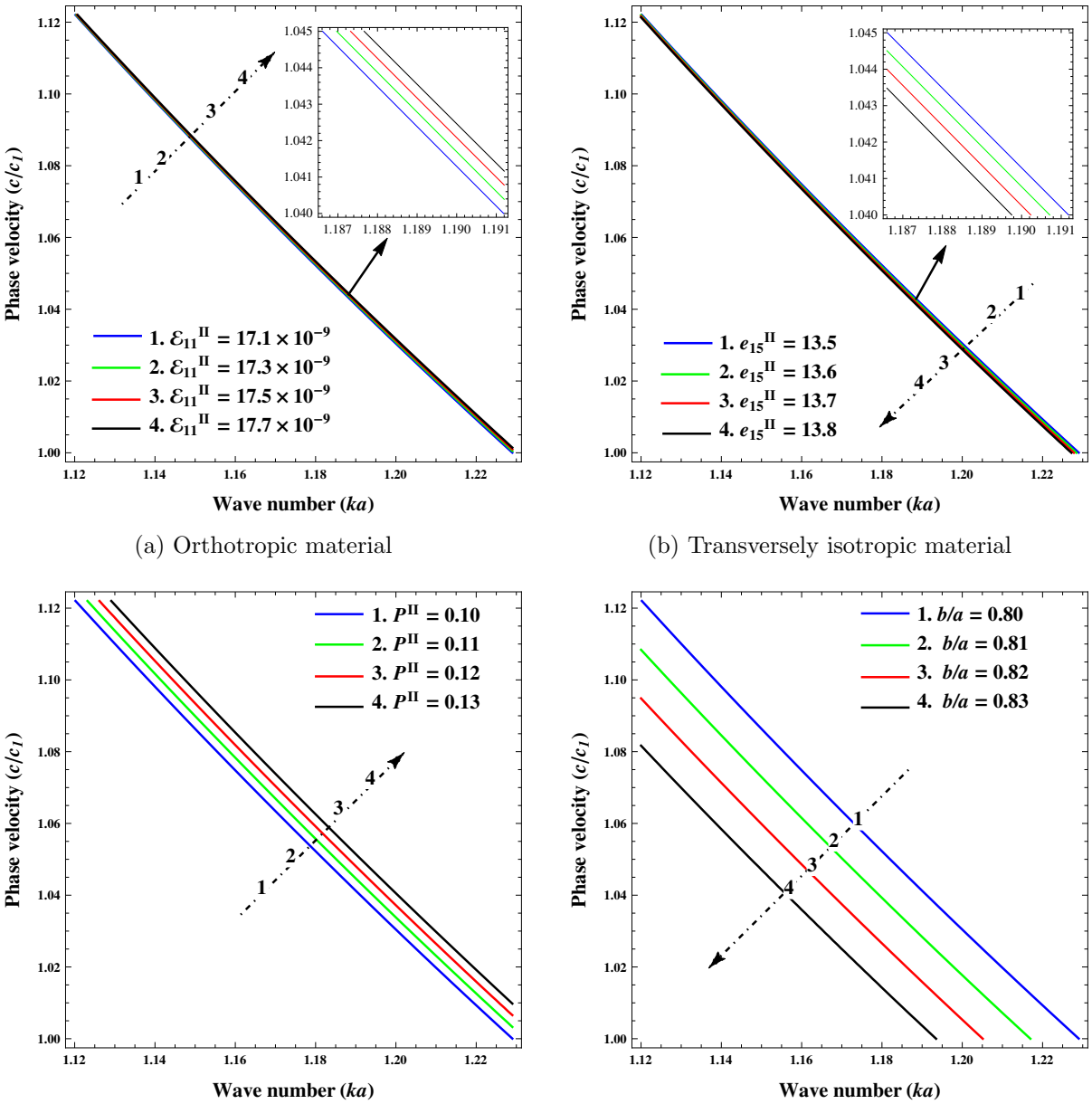
(d) Comparison of all materials

Figure 3: Phase velocity variation (c/c_1) versus wave number (ka) in the case of imperfect interfaces, an transversely isotropic (zinc) coating for different values of (a) dielectric constant (ε_{11}^{II}), (b) piezoelectric constant (e_{15}^{II}), (c) initial stress (P^{II}), and (d) radii ratio (b/a).

well as there is increased wave confinement in the coated layer.

7.2 Effects on the phase velocity for zinc imperfect coating

The influence of (a) the dielectric parameter (ε_{11}^{II}), (b) the piezoelectric constant (e_{15}^{II}), (c) the initial stress (P^{II}), and (d) the radii ratio (b/a) on the phase velocity in an imperfectly bonded zinc (transversely isotropic) coating is shown in Figure 3. Figures 3(a) and 3(c) reveal that the phase velocity grows with an increase in e15 and P2. The larger value of the piezoelectric parameter implies the stronger electromechanical coupling, while the initial stress increases the effective stiffness of the medium; thus, the wave propagates faster. On the contrary, the phase velocity decreases with an increase in E11 and radii ratio according to Figures 3(b) and 3(d). An increase in the dielectric parameter decreases the strength of the electromechanical



(a) Orthotropic material

(b) Transversely isotropic material

(c) Isotropic material

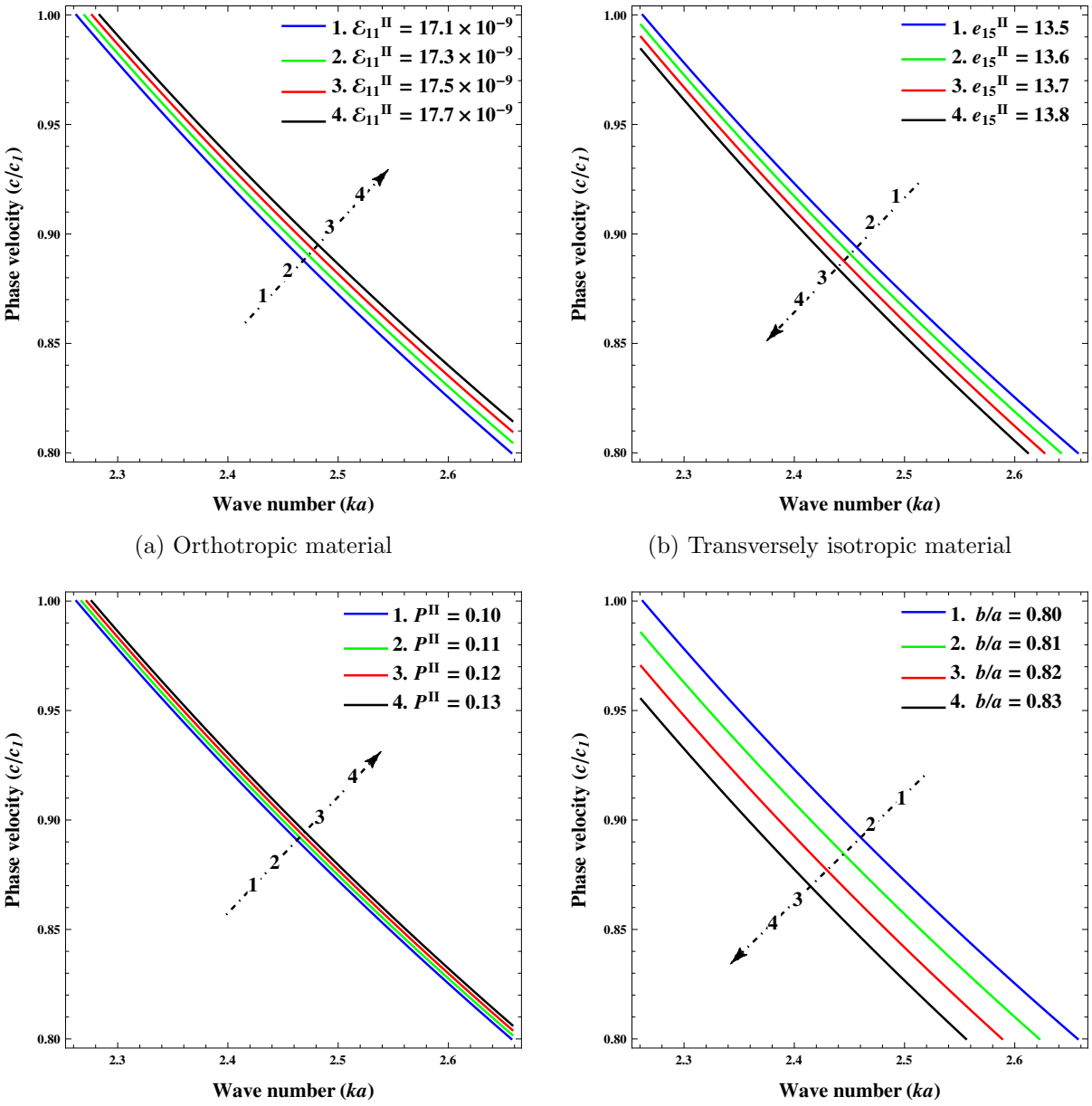
(d) Comparison of all materials

Figure 4: Phase velocity variation (c/c_1) versus wave number (ka) in the case of imperfect interfaces, simply isotropic coating for different values of (a) dielectric constant (ε_{11}^{II}), (b) piezoelectric constant (e_{15}^{II}), (c) initial stress (P^{II}), and (d) radii ratio (b/a).

coupling; meanwhile, an increase in the radii ratio decreases the effective stiffness because the relative coating thickness grows; thus, the phase velocity reduces. Even though the influence of the above-mentioned parameters on the phase velocity is monotonous, the influence of the dielectric and piezoelectric parameters is negligibly small.

7.3 Effects on the phase velocity for isotropic imperfect coating

Figure 4 represents the effect of (a) dielectric parameter (ε_{11}^{II}), (b) piezoelectric constant (e_{15}^{II}), (c) initial stress (P^{II}), and (d) radii ratio (b/a) on the normalized phase velocity for an isotropic coating with imperfect bonding. It is evident from Figs. 4(a) and 4(c) that phase velocity is an increasing function of dielectric parameter and initial stress. An increase in dielectric parameter



(a) Orthotropic material

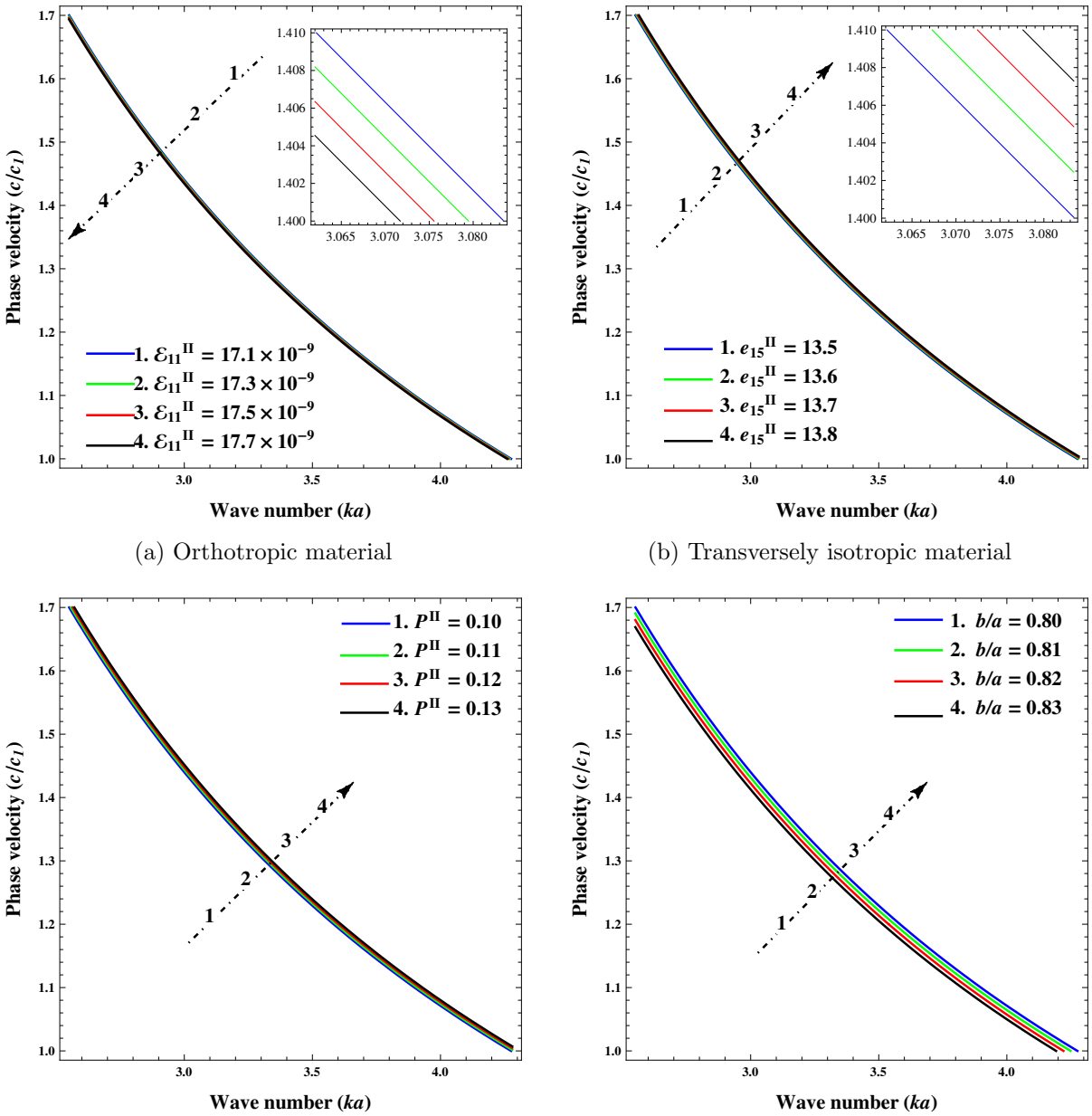
(b) Transversely isotropic material

(c) Isotropic material

(d) Comparison of all materials

Figure 5: Phase velocity variation (c/c_1) versus wave number (ka) in the case of perfect interfaces, an orthotropic (epoxy-graphite) coating for different values of (a) dielectric constant (ε_{11}^{II}), (b) piezoelectric constant (e_{15}^{II}), (c) initial stress (P^{II}), and (d) radii ratio (b/a).

means enhancement in the ability of energy storage in the electrical field of material. On the other hand, initial stress increases the stiffness of the material; therefore, there will be slight increment in the phase velocity. However, Fig. 4(b) shows that with increasing piezoelectric parameter, there is slight decrement in phase velocity due to modification in electromechanical coupling. An increase in radii ratio results in an increase in relative thickness of coating which reduces the stiffness of the coated layer, hence phase velocity decreases with increasing radii ratio. The effect of dielectric and piezoelectric parameters is minor while effect of radii ratio is significant.



(a) Orthotropic material

(b) Transversely isotropic material

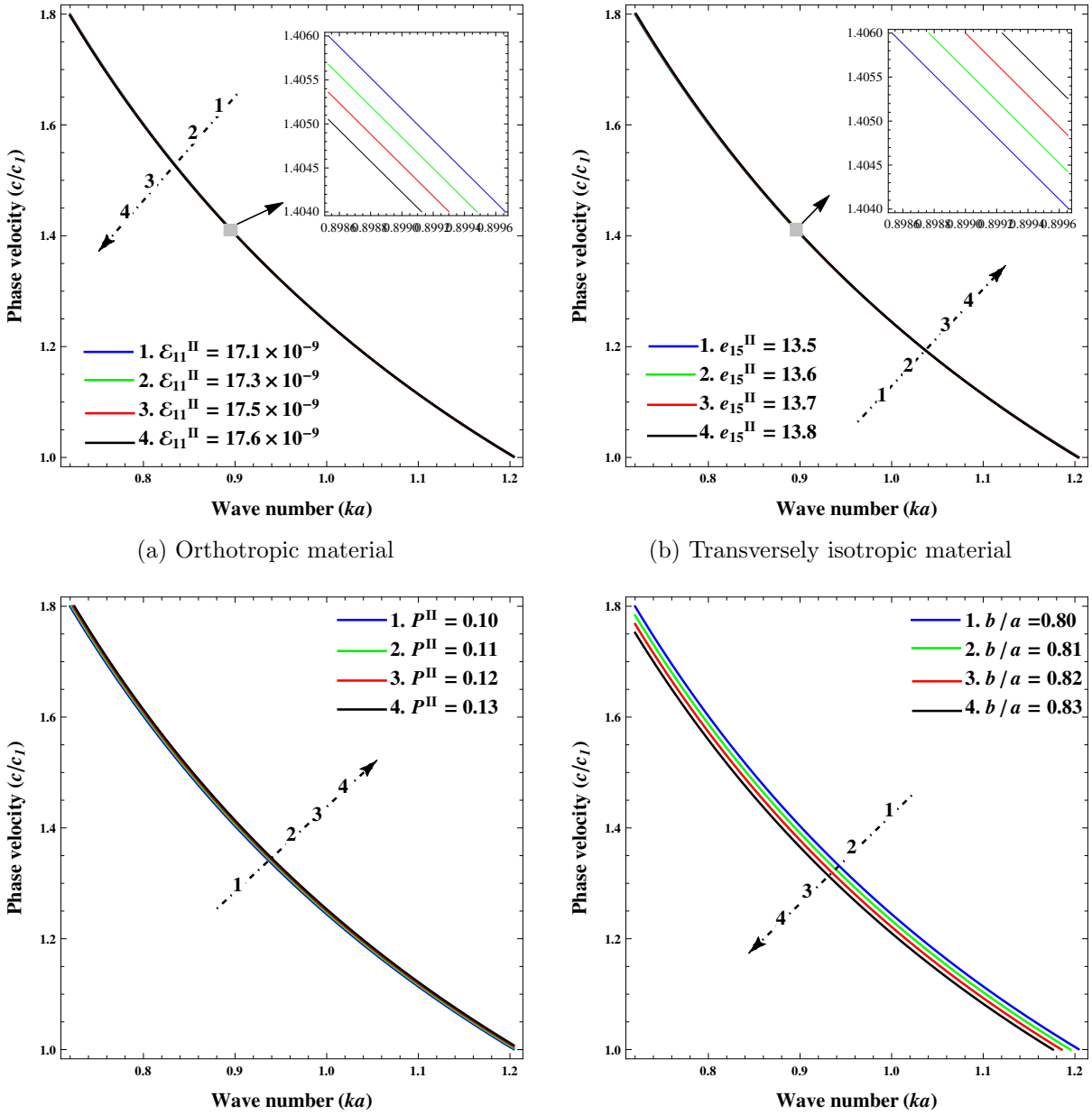
(c) Isotropic material

(d) Comparison of all materials

Figure 6: Phase velocity variation (c/c_1) versus wave number (ka) in the case of perfect interfaces, transversely isotropic (zinc) coating for different values of (a) dielectric constant (ε_{11}^{II}), (b) piezoelectric constant (e_{15}^{II}), (c) initial stress (P^{II}), and (d) radii ratio (b/a).

7.4 Effects on the phase velocity for epoxy-graphite perfect coating

The effect of (a) the dielectric parameter (ε_{11}^{II}), (b) the piezoelectric constant (e_{15}^{II}), (c) the initial stress parameter (P^{II}), and (d) the radii ratio (b/a) on the normalized phase velocity for a perfectly bonded orthotropic epoxy-graphite coating is shown in Figure 5. In all cases, an increase in the wave number results in a decrease in the phase velocity, suggesting the dispersive nature of SH-waves. From Figures 5(a) and 5(c), we observe that an increase in the phase velocity occurs as the value of the dielectric parameter and initial stress increases. The higher value of the dielectric parameter implies increased energy storage capacity due to the electrical fields in the medium, while the initial stress affects the stiffness of the medium by increasing its value. On the other hand, Figures 5(b) and 5(d) demonstrate that an increase in the phase



(a) Orthotropic material

(b) Transversely isotropic material

(c) Isotropic material

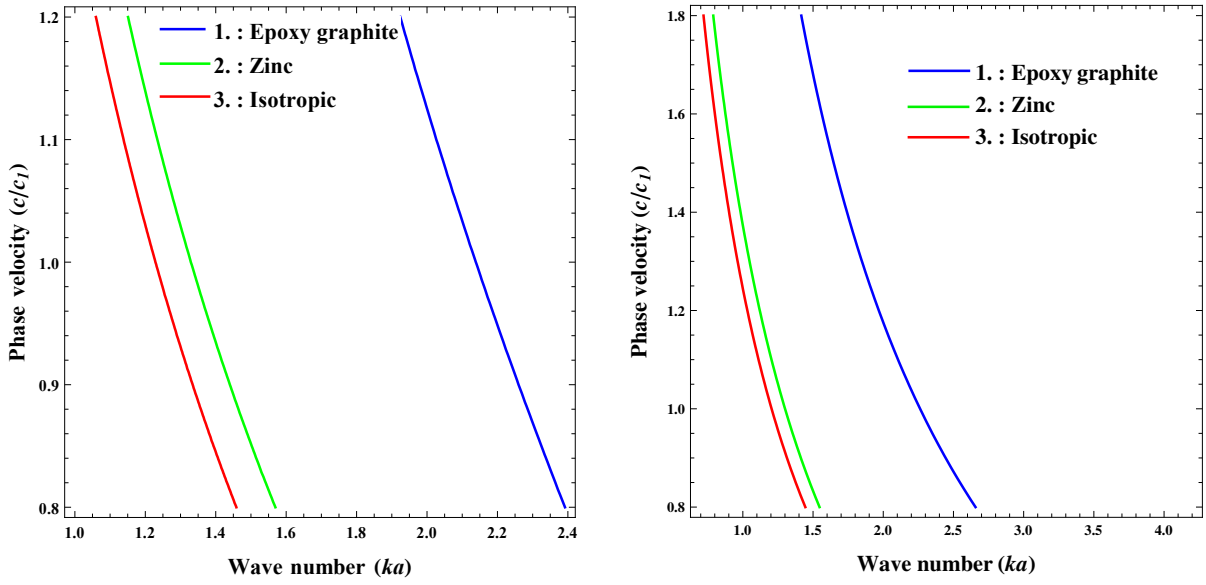
(d) Comparison of all materials

Figure 7: Phase velocity variation (c/c_1) versus wave number (ka) in the case of perfect interfaces, simply isotropic coating for different values of (a) dielectric constant (ε_{11}^{II}), (b) piezoelectric constant (e_{15}^{II}), (c) initial stress (P^{II}), and (d) radii ratio (b/a).

velocity causes a decrease in the values of piezoelectric constant and radii ratio. An increase in the piezoelectric constant influences the coupling between electrical and mechanical fields, causing the phase velocity to decrease slightly, while the larger radii ratio indicates increased coating thickness.

7.5 Effects on the phase velocity for zinc perfect coating

Figure 6 demonstrates the effect of (a) dielectric parameter (ε_{11}^{II}), (b) piezoelectric constant (e_{15}^{II}), (c) initial stress parameter (P^{II}), and (d) radii ratio (b/a) on the normalized phase velocity of a perfectly bonded zinc (transversely isotropic) coating. In all four cases, the phase velocity is decreasing nonlinearly with increasing wave number, which shows the dispersive



(a) (b)

Figure 8: Phase velocity variation (c/c_1) versus wave number (ka) for epoxy-graphite (orthotropic), zinc (transversely isotropic), and isotropic coatings under (a) imperfect and (b) perfect interface.

behavior of SH-waves. Figures 6(b) and 6(c) demonstrate an increase in the phase velocity with an increase in piezoelectric constant and initial stress, respectively. An increase in piezoelectric constant results in the increased strength of electromechanical interaction, whereas an increase in initial stress increases the effective stiffness of the medium, and hence results in an increase in phase velocity. Figures 6(a) and 6(d) demonstrate the decreasing behavior of the phase velocity with an increase in dielectric parameter and radii ratio, respectively. An increase in dielectric parameter increases the electrical energy storing capacity of the material and hence reduces the effective electromechanical interaction, whereas the increase in radii ratio increases the effective thickness of the coating and consequently reduces the effective stiffness of the coated medium. The effect of dielectric and piezoelectric parameters is comparatively small, whereas the effect of radii ratio is the largest one.

7.6 Effects on the phase velocity for isotropic perfect coating

Figure 7 shows the effects of (a) the dielectric constant (ε_{11}^{II}), (b) the piezoelectric constant (e_{15}^{II}), (c) the initial stress (P^{II}), and (d) the radii ratio (b/a) on the normalized phase velocity of the perfectly bonded isotropic coating. It can be seen that the phase velocity in all cases decays nonlinearly with increasing wave number due to dispersive behavior of SH-waves in the composite structure. Figs. 7(b) and 7(c) show that the phase velocity rises with increasing piezoelectric constant and initial stress. The rise in piezoelectric constant improves the electromechanical coupling, and the increase in initial stress increases the stiffness of the medium, which results in fast wave propagation. However, Fig. 7(a) and 7(d) illustrate that the phase velocity declines with increasing dielectric constant and radii ratio. The increase in the dielectric constant increases the ability of the material to store electrical energy, resulting in weak effective electromechanical coupling. On the other hand, an increase in the radii ratio increases the relative thickness of the coating, hence decreasing the stiffness of the coated structure, and as a consequence, decreases the phase velocity. The effect of the dielectric and piezoelectric constants is less pronounced, whereas the radii ratio is the most significant one.

7.7 Comparative analysis of phase velocity considering imperfect and perfect interface conditions based on materials properties

Figure 8 presents a comparative study of the phase velocity of the waves that propagate in orthotropic epoxy-graphite, transversely isotropic zinc, and isotropic coatings for imperfect and perfect interface conditions. As seen in Figure 8, the phase velocity decreases as the wave number increases in both cases, demonstrating the wave's dispersive behavior. For the three types of materials, it can be noticed that orthotropic epoxy-graphite coating possesses a greater value of phase velocity in comparison to transversely isotropic zinc and isotropic coatings throughout the range of wave number. The reason behind the above-mentioned trend lies in the fact that orthotropic epoxy-graphite material has high effective stiffness and anisotropic properties, allowing faster wave propagation. Perfect interface provides a greater value of phase velocity than the imperfect interface due to better continuity of displacements and stresses at the interface.

8 Conclusion

This study is focused on the propagation behavior of SH-waves in the composite cylinder made up of piezoelectric material and having orthotropic, transversely isotropic, and isotropic coating under the conditions of imperfect and perfect interfaces. The present study includes the derivation of analytical dispersion equation to investigate the role of dielectric constant, piezoelectric constant, initial stress, radii ratio, interface condition, and anisotropy of materials in the phase velocity. The following are the main results of the current investigation:

- Phase velocity decreases with an increase in the wave number for all material models and interface conditions; the dispersive behavior of SH-waves is thus validated.
- The phase velocity is significantly increased by the piezoelectric constant due to the enhanced electromechanical interaction between the two phases, but the dielectric constant plays a minor role in this regard.
- An increase in the initial stress causes an increase in the stiffness of the medium and therefore an increase in the phase velocity, but an increase in the radius ratio causes a decrease in the phase velocity because of the relatively thick coating.
- Perfect interface conditions give rise to higher phase velocities compared to imperfect interface conditions due to better continuity of displacement and stress at the interface, resulting in better wave propagation.
- Among the three coatings considered, the orthotropic epoxy-graphite coating provides the highest phase velocity, followed by the transversely isotropic zinc coating, while the isotropic coating provides the lowest phase velocity, thereby highlighting the importance of material anisotropy in wave propagation.
- The sensitivity analysis reveals that the radii ratio and interface condition have a greater effect on phase velocity than the dielectric parameter, while the effect of the piezoelectric parameter is relatively low in all cases.
- The developed analytical model and the results obtained can provide a useful guide for the design and optimization of piezoelectric waveguides, ultrasonic sensors and actuators, SAW and BAW devices, SHM systems, NDE techniques, vibration control systems, energy harvesting systems, and aerospace and automotive composites, where accurate modeling and control of wave propagation are required.

Acknowledgment

The authors gratefully acknowledge the financial support provided by the Anusandhan National Research Foundation (ANRF), Government of India (Project File No. TAR/2023/000174), for facilitating this research. The authors also sincerely thank VIT University, Vellore, for their support and infrastructure provided during the course of this work.

Conflict of interest

The authors declare no Conflict of interest.

References

[1] J. Curie and P. Curie, "Développement par compression de l'électricité polaire dans les cristaux hémièdres à faces inclinées," *Comptes Rendus de l'Académie des Sciences*, 1880.

[2] M. Jaffe, B. Jaffe, and W. R. C. Jr., *Piezoelectric Ceramics*. Academic Press, 1971.

[3] A. Safari and E. K. Akdogan, *Piezoelectric and Acoustic Materials for Transducer Applications*. Springer, 2008.

[4] B. Jaffe, W. R. C. Jr., and H. Jaffe, *Piezoelectric Ceramics*. Academic Press, 1971.

[5] R. Martins, A. Nathan, N. Barros, and E. Fortunato, *Flexible Electronics: Materials and Applications*. Wiley, 2011.

[6] C. Sirohi and I. Chopra, "Smart materials and structures," *Smart Materials and Structures*, 2000.

[7] S. Priya and D. J. Inman, *Energy Harvesting Technologies*. Springer, 2009.

[8] Z. L. Wang and J. Song, "Piezoelectric nanogenerators based on zinc oxide nanowire arrays," *Science*, vol. 312, no. 5771, pp. 242–246, 2006.

[9] H. Uchino, *Advanced Piezoelectric Materials: Science and Technology*. Woodhead Publishing, 2010.

[10] S. Bauer, R. Gerhard-Multhaupt, and G. M. Sessler, "Ferroelectrets: Soft electroactive foams for transducers," *Nature Materials*, vol. 13, no. 10, pp. 1015–1026, 2014.

[11] Z. L. Wang, "Progress in piezotronics and tribotronics," *Nano Energy*, vol. 1, no. 1, pp. 13–24, 2012.

[12] Y. Saito, H. Takao, T. Tani, T. Nonoyama, K. Takatori, T. Homma, T. Nagaya, and M. Nakamura, "Lead-free piezoceramics," *Nature*, vol. 432, pp. 84–87, 2004.

[13] K. Uchino, "History of piezoelectric materials and their applications," *Journal of Materials Science: Materials in Electronics*, vol. 26, pp. 4424–4435, 2015.

[14] T. Li and Y. Wang, "Propagation characteristics of sh wave in orthotropic layer/piezoelectric column structure," in *Journal of Physics: Conference Series*, vol. 2381, no. 1. IOP Publishing, 2022, p. 012070.

[15] Y. Jiang, C. Zhou, B. Wang, and L. Wu, "Magnetoelastic coupled wave diffraction and dynamic stress intensity factor in graded piezomagnetic composites with a cylindrical aperture," *Materials*, vol. 13, no. 3, p. 669, 2020.

[16] P. Alam, T. Nahid, B. Al Alwan, and A. Saha, "Rotating radial vibrations in human bones (femoral, mandibular and tibia) and crystals (mg, co, cd, zn and beryl) made cylindrical shell under magnetic field and hydrostatic stress," *Mechanics of Advanced Materials and Structures*, vol. 30, no. 13, pp. 2684–2700, 2023.

[17] K. Pankaj, S. Sahu, and S. Kumari, "Surface wave transference in a piezoelectric cylinder coated with reinforced material," *Applied Mathematics and Mechanics*, vol. 41, no. 1, pp. 123–138, 2020.

[18] M. Arif and P. Alam, "Study of circumferential sh-wave interaction with a piezoelectric cylinder having pre-stressed viscoelastic imperfect coating," *Mechanics Research Communications*, vol. 141, p. 104323, 2024.

[19] S. Pengpeng, X. Jun, and H. Shuai, "Static response of functionally graded piezoelectric-piezomagnetic hollow cylinder/spherical shells with axial/spherical symmetry," *Journal of Mechanical Science and Technology*, vol. 35, no. 4, pp. 1583–1596, 2021.

[20] P. Alam, S. Manam *et al.*, "Circumferential interaction of shear waves with doubly piezomagnetic materials made cylindrical structure," *Applied Physics A*, vol. 131, no. 7, pp. 1–16, 2025.

[21] Seema, M. Alamoudi, A. M. Saeed, R. A. Alahmadi, A. Chaudhary, and A. H. Ganie, "Shear–horizontal wave transmission in prestressed rotating piezoelectric–piezomagnetic cylinders with imperfect interfaces: analytical modeling and parametric insights," *Acta Mechanica*, pp. 1–21, 2025.

[22] X. Wang, E. Pan, and A. Roy, "Scattering of antiplane shear wave by a piezoelectric circular cylinder with an imperfect interface," *Acta mechanica*, vol. 193, no. 3, pp. 177–195, 2007.

[23] A. E. H. Love, *A Treatise on the Mathematical Theory of Elasticity.* New York: Dover Publications, 1944.

[24] J. D. Achenbach, *Wave Propagation in Elastic Solids.* Amsterdam: North-Holland Publishing Company, 1973.

[25] L. Thomsen, "Weak elastic anisotropy," *Geophysics*, vol. 51, no. 10, pp. 1954–1966, 1986.

[26] J. M. Carcione, *Wave Fields in Real Media: Wave Propagation in Anisotropic, Anelastic, Porous and Electromagnetic Media.* Elsevier, 2007.

[27] M. J. P. Musgrave, *Crystal Acoustics: Introduction to the Study of Elastic Waves and Vibrations in Crystals.* San Francisco: Holden-Day, 1970.

[28] A. Bedford and D. S. Drumheller, *Introduction to Elastic Wave Propagation.* John Wiley & Sons, 1994.

[29] P. Alam, S. Kundu, and S. Gupta, "Propagation of love-type waves emanating due to a disturbance point source in a transversely isotropic layer under initial stress and magnetic field over an inhomogeneous half-space," *Journal of Applied and Computational Mechanics*, vol. 8, no. 3, pp. 911–921, 2022.

[30] A.-e.-n. N. Abd-alla, A. Raizah, and L. Placidi, "The influence of hydrostatic stress on the frequency equation of flexural waves in a magnetoelastic transversly isotropic circular cylinder," *ZAMM-Journal of Applied Mathematics and Mechanics/Zeitschrift für Angewandte Mathematik und Mechanik*, vol. 96, no. 1, pp. 53–66, 2016.

[31] M. A. Biot, *Mechanics of Incremental Deformations: Theory of Elasticity and Viscoelasticity of Initially Stressed Solids and Fluids, Including Thermodynamic Foundations and Applications to Finite Strain*. New York: John Wiley & Sons, 1965.

[32] R. G. Payton, *Elastic Wave Propagation in Transversely Isotropic Media*. Berlin, Germany: Springer, 1983.

[33] D. Gubbins, *Seismology and Plate Tectonics*. Cambridge: Cambridge University Press, 1990.

[34] D. Berlincourt, D. R. Curran, and H. Jaffe, "Piezoelectric and piezomagnetic materials," in *Physical Acoustics, Volume 1A*, W. P. Mason, Ed. New York: Academic Press, 1964, pp. 169–270.